PROCEEDINGS OF SPIE

SPIEDigitalLibrary.org/conference-proceedings-of-spie

Experimental measurements of AO-fed photonic lantern coupling efficiencies

Jonathan Lin, Sebastian Vievard, Nemanja Jovanovic, Barnaby Norris, Michael P. Fitzgerald, et al.

Jonathan Lin, Sebastian Vievard, Nemanja Jovanovic, Barnaby Norris, Michael P. Fitzgerald, Christopher Betters, Pradip Gatkine, Olivier Guyon, Yoo Jung Kim, Sergio Leon-Saval, Julien Lozi, Dimitri Mawet, Steph Sallum, Yinzi Xin, "Experimental measurements of AO-fed photonic lantern coupling efficiencies," Proc. SPIE 12188, Advances in Optical and Mechanical Technologies for Telescopes and Instrumentation V, 121882E (29 August 2022); doi: 10.1117/12.2630608

SPIE.

Event: SPIE Astronomical Telescopes + Instrumentation, 2022, Montréal, Québec, Canada

Experimental Measurements of AO-Fed Photonic Lantern Coupling Efficiencies

Jonathan Lin[a], Sebastien Vievard[b], Nemanja Jovanovic[c], Barnaby Norris[d], Michael P. Fitzgerald[a], Christopher Betters[e], Pradip Gatkine[c], Oliver Guyon[b,f], Yoo Jung Kim[a], Sergio Leon-Saval[e], Julien Lozi[b], Dimitri Mawet[c], Steph Sallum[g], and Yinzi Xin[c]

[a]Physics & Astronomy Department, University of California, Los Angeles (UCLA), 475 Portola Plaza, Los Angeles, USA
[b]Subaru Telescope, 650 N. A'ohoku Place, Hilo, HI 96720 USA
[c]Department of Astronomy, California Institute of Technology, 1200 E. California Blvd, Pasadena, USA
[d]Sydney Institute for Astronomy, School of Physics, Physics Road, The University of Sydney, NSW 2006, Australia
[e]Sydney Astrophotonic Instrumentation Laboratory, School of Physics, The University of Sydney, Sydney, NSW 2006, Australia
[f]University of Arizona Steward Observatory, Tucson, AZ 85721, USA
[g]Department of Physics & Astronomy, University of California, Irvine, 4129 Frederick Reines Hall, Irvine, CA 92697 USA

ABSTRACT

Efficiently coupling light from large telescopes to photonic devices is challenging. However, overcoming this challenge would enable diffraction-limited instruments, which offer significant miniaturization and advantages in thermo-mechanical stability. By coupling photonic lanterns with high performance adaptive optics systems, we recently demonstrated through simulation that high throughput diffraction-limited instruments are possible (Lin et al., Applied Optics, 2021). Here we build on that work and present initial results from validation experiments in the near-infrared to corroborate those simulations in the laboratory. Our experiments are conducted using a 19-port photonic lantern coupled to the state-of-the-art SCExAO instrument at the Subaru Telescope. The SCExAO instrument allows us to vary the alignment and focal ratio of the lantern injection, as well as the Strehl ratio and amount of tip/tilt jitter in the beam. In this work, we present experimental characterizations against the aforementioned parameters, in order to compare with previous simulations and elucidate optimal architectures for lantern-fed spectrographs.

Keywords: Astrophotonics, High-resolution spectroscopy, Photonic lantern, Diffraction-limited spectroscopy

1. INTRODUCTION

Diffraction-limited spectrographs fed by single-mode fibers (SMFs) offer advantages over seeing-limited spectrographs in both compactness and thermo-mechanical stability,[1,2] and are quickly becoming the preferred architecture in spectrograph design. However, the coupling of large telescopes into SMF-fed spectrographs has historically been challenging due to the mismatch between the Gaussian-like fundamental mode of the fiber, and the telescope point-spread function (PSF), which is unstable due to time-varying wavefront error (WFE) originating from both atmospheric turbulence and the instrument itself.

The photonic lantern (PL) is a tapered waveguide which can efficiently couple light from a few-mode fiber (FMF) into multiple single-mode outputs.[3,4] This device represents an alternate way to inject telescope light

Further author information: (Send correspondence to Jonathan Lin)
Jonathan Lin: E-mail: jon880@astro.ucla.edu

Advances in Optical and Mechanical Technologies for Telescopes and Instrumentation V, edited by Ramón Navarro, Roland Geyl, Proc. of SPIE Vol. 12188, 121882E
© 2022 SPIE · 0277-786X · doi: 10.1117/12.2630608

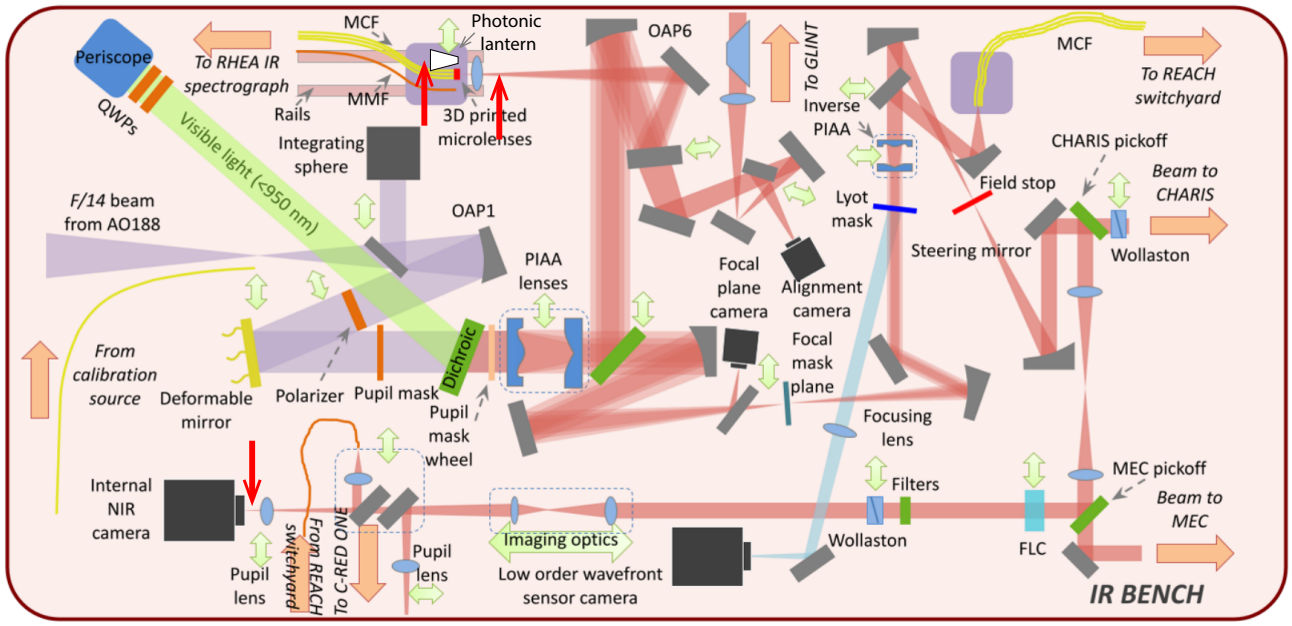

Figure 1. Diagram of the SCExAO IR test bench. Adapted from 11. The photonic lantern is located in the top left, mounted on a 5-axis translation stage. Also on the stage is an SMF, which was used for NCPA calibrations. The three red arrows denote locations where power meter measurements were taken.

into SMF-fed spectrographs. Notably, initial simulations[5] have shown that lantern-based injection systems may offer significant benefits in coupling efficiency over traditional SMF-fed injection. However, while simulations are undoubtedly a crucial first step in characterizing the coupling performance of the PL, they should not be the only step. The challenge in performing a simulation that is truly representative of real physics is two-fold. For one, real lanterns, due to quirks in the fabrication process, may look significantly different (and thus behave differently) than the ideal lanterns assumed in simulations. This is especially the case for lanterns made by stacking and tapering bundles of SMFs: claddings for such lanterns at the FMF end may look more flower-shaped than circular (e.g. Figure 6 from 6). Additionally, realistic WFE, which includes the effect of atmospheric turbulence, non-common path aberrations (NCPAs; 7, 8), tip-tilt jitter, and the island effect,[9,10] is difficult to simulate. These challenges motivate the need for experimental validation and characterization of the PL.

In this work we present initial results from our ongoing experiments in the near-infrared (NIR) to characterize the 19-port PL on the SCExAO instrument[11] at the Subaru Telescope. An overview of SCExAO's IR bench is shown in Figure 1. We now go over the relevant optical components for the experiments covered in this work. Light is first emitted from a supercontinuum calibration source, and passes through a 1550 $\pm$ 25 nm filter placed in the source box. This light is collimated by an off-axis parabolic (OAP) mirror, and then sent to a 2,000 actuator deformable mirror (DM). Light then passes through a set of phase-induced amplitude apodization (PIAA) lenses, which reformat the beam to be Gaussian in amplitude, thereby removing Airy rings in the focal plane.[12] After the PIAA optics, the bulk of the light is picked off, and then sent to the PL via another OAP and a focusing lens. The PL is mounted on a translation stage (we will call this the "injection stage") which can move in x, y, f, and z. The first two coordinates control the alignment of the stage transverse to the optical beam, while the latter two coordinates can be adjusted to change the focal ratio of the injection (for more details see[13]). The output of the lantern, which looks like a multicore fiber (MCF), is imaged by the GLINT[14] detector (a FirstLight Imaging C-red2, InGaAs detector). Meanwhile, the light not sent to the lantern is ultimately directed to SCExAO's internal NIR camera (bottom left of Figure 1). In Section §2, we provide an overview of the experimental procedures used to collect data from the 19-port PL on SCExAO. In §3, we present the results of these tests, and compare them to numerical models from 5. Finally, in §4 we discuss our results, and lay a course for future experiments.

2. METHOD

In this work, we present three different types of characterizations in relative throughput and one preliminary measurement of absolute throughput for the 19-port PL on SCExAO. All measurements were taken off-sky. We first go over some initial preparations we took before beginning our main data collection, and then detail the experimental setup for each set of measurements.

2.1 Preparations

Before taking measurements with the PL, we first aligned the stage in x, y, f, and z for optimal coupling into the Corning SMF-28 fiber mounted on the same translation stage as the PL. Our reason for this is two-fold: first, because SMFs only accept light that is flat in phase, we can modulate the DM and monitor SMF coupling in order to construct an NCPA compensation map. Second, coupling efficiencies of the same SMF were experimentally measured previously by 13; repeating these measurements will improve confidence in our subsequent measurements with the PL.

We first correct for non-common-path aberrations (NCPAs) between the GLINT lightpath and the SCExAO internal NIR camera lightpath. Using the DM, we then scan over the first 10 non-piston Zernike modes, monitoring the effect on coupling efficiency. For each mode, we record the mode amplitude which maximized SMF coupling; this list of mode amplitudes is then converted to a phase map which we apply to the DM for NCPA compensation.

With NCPA compensation applied, we then used a power meter to measure fluxes before and after the injection stage, in order to estimate the absolute coupling efficiency into the SMF. This efficiency was measured before by 13 to be $\sim 87\%$; we recover a value of 83 $\pm 3\%$, which is lower than the previous measurement but still close. Note that both estimates are solely of coupling efficiencies: losses due to Fresnel reflection and lens transmission are accounted for and divided out.

After our tests with the SMF, we realigned the system solely in x and y to maximize coupling into the PL, then moved on to PL characterization, detailed below.

2.2 Throughput vs. xy

For this test, we simply put the PL into focus and then shift the stage in x and y while recording the flux measured by the GLINT detector and the internal NIR camera detector. We then take the ratio of these two measurements: this proxy metric should be proportional to absolute lantern throughput, with the added benefit of being immune to variability in the supercontinuum source. After collecting a set of flux ratios, we divide by the largest value to scale our data relative to the maximum measured throughput.

We also maintain a focal ratio of 4.3: this was the optimal focal ratio for injection into the SMF mounted next to the PL, for our nominal wavelength of 1550 nm. According to simulations, $f/4.3$ should also be close to optimal for the 19-port PL, even though the resulting PSF will be undersized compared to the lantern's mode field diameter (MFD). This claim is also corroborated by our throughput vs. focal ratio measurements, covered in the next subsection. Note that converting the f and z coordinates of the injection stage position into a focal ratio is non-trivial: our approach is outlined in Appendix A. Note that the NCPA map mentioned in 2.1 was not applied; however, because the PSF is undersized compared to the lantern MFD, it is unlikely that NCPA corrections will make a significant difference. We apply NCPA correction for later tests.

2.3 Throughput vs. focal ratio

For this test, apply our NCPA correction on the FM and scan the injection stage over z. For each z we align the PL in x, y, and f, then measured a flux ratio in the same manner as the previous subsection. We also scale these flux ratios relatively, as in the previous subsection.

2.4 Throughput vs. Strehl ratio

In this test we apply our NCPA compensation map to the DM and align the PL, setting the focal ratio to 4.3. We then artificially introduce WFE to the system. This WFE, which is produced by the turbulence simulator on the SCExAO real-time computer (RTC) and played back by the DM, is primarily Kolmogorov in nature, but with power in the low spatial frequencies suppressed in order to emulate partial correction of the wavefront by the AO188 system, Subaru Telescope's facility AO system. To characterize how relative throughput depends on Strehl ratio, we ramp up this simulated WFE, and for each Strehl, record 100 flux ratios. PSF images from the internal NIR camera are used to manually calculate Strehl ratio.

We later repeat this characterization, but increase the relative proportion of low-order wavefront error. This is done by changing the value of the "low-order coefficient" parameter in the turbulence simulator from 0.01 (the default value) to 1.

2.5 Absolute throughput measurement

In this subsection we detail our procedure for estimating the absolute throughput of the 19-port PL. After applying NPCA compensation, we aligned the injection stage in x and y for the PL (keeping the same 4.3 focal ratio) and then took four sets of three power meter measurements, the locations of which are indicated by the three red arrows in Figure 1. Our measurements and the corresponding estimate of the PL throughput are summarized in subsection §3.4.

3. RESULTS

3.1 Throughput vs. xy

Figure 2 (left) shows the throughput map produced from the experimental procedure outlined in subsection §2.2. Interestingly, we find that the relative throughput varies by a factor of up to 3 over the face of the lantern, and note that the throughput pattern is stable, at least on the order of several days. This is already a deviation from simulation: for comparison, Figure 2 (right) shows the simulated coupling efficiency of the SCExAO PSF (accounting for the effect of PIAA optics) into an FMF matching the dimensions of the PL entrance. This coupling map is flat over the entrance of the fiber. Note that coupling efficiency is not the same as throughput: coupling efficiency accounts only for light loss that occurs at the FMF-like entrance of the lantern, while throughput additionally accounts for loss during propagation through the lantern transition. However, the former is often taken as a proxy for the latter because internal losses for PLs are usually assumed to be low. In fact, PLs with internal losses of only a few % have experimentally demonstrated.[15,16]

3.2 Throughput vs. focal ratio

Figure 3 compares measured relative throughput of the 19-port PL (black points) against the simulated coupling efficiency into an FMF whose core diameter matches the size of the lantern entrance (dotted blue), over a range of focal ratios. We note decent agreement between experimental results and simulation, except at around $f/10$. Interestingly, at this focal ratio, the size of the PSF should roughly match the MFD of the PL; however, experiment and simulation both show that throughput/coupling efficiency at $\sim f/10$ is slightly lower than the maximal value at $\sim f/5$, suggesting that optimal coupling occurs when the PSF is undersized compared to the lantern MFD.

3.3 Throughput vs. Strehl ratio

Figure 4 shows the results of our tests described in subsection §2.4. Blue points show experimentally measured relative throughputs of the PL, as a function of Strehl, while the black dashed line shows the simulated relative coupling efficiency of an aberrated beam into a similarly sized FMF. For simulations, WFE was produced by simulating a closed-loop AO system which partially corrects a single layer of Kolmogorov turbulence; Strehl is tuned by adjusting the Fried parameter, r_0. For more detail, refer to the method for WFE simulation described in 5. Our experiment recovers a linear relation between throughput and Strehl ratio, as expected from simulation; however, the slopes of the measured and simulated relations differ slightly. At our current stage of

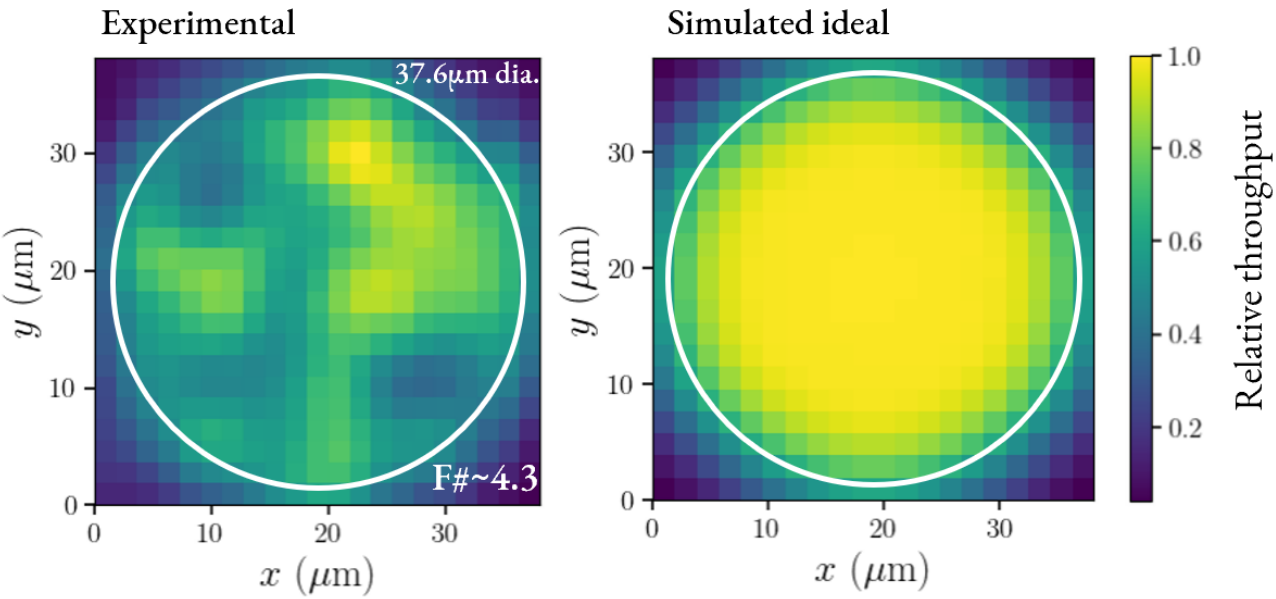

Figure 2. Left: total measured throughput of the 19-port PL, scaled against the maximum measured throughput, as a function of xy position. The cladding-jacket interface (37.6 μm diameter) is outlined in white. The focal ratio was set to 4.3. Right: simulated coupling efficiency, at the same focal ratio, between the SCExAO PSF and a few-mode step-index optical fiber that matches the entrance geometry of the PL.

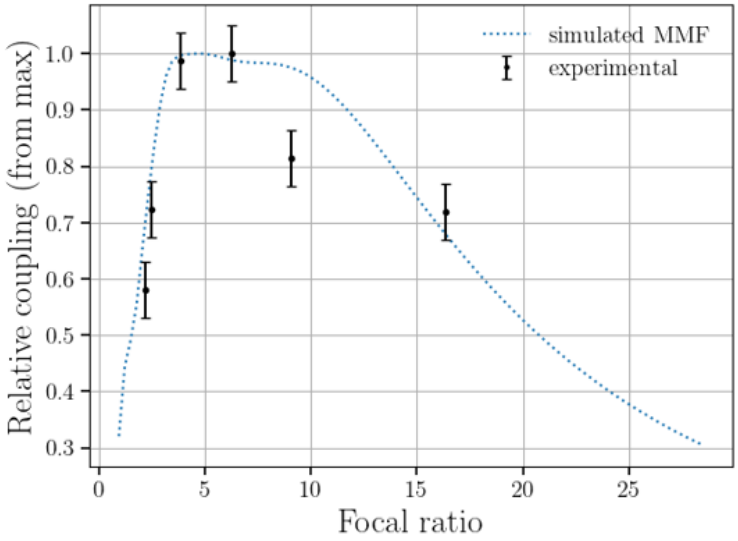

Figure 3. Black: net throughput of the 19-port PL, for various focal ratios. Blue: simulated coupling efficiency between the SCExAO PSF and an FMF matching the dimensions of the lantern entrance. Agreement is good except for around $f/10$.

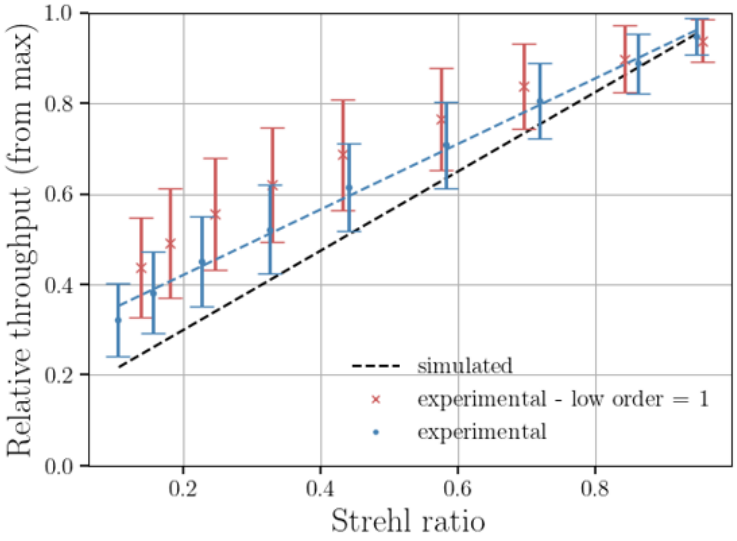

Figure 4. Blue: measured (relative) net throughput of the 19-port PL as a function of Strehl ratio. Strehl is altered by adjusting the amplitude of the WFE produced by the turbulence simulator on the SCExAO RTC. For each Strehl we measure relative throughput 100 times: points and bars show the mean and standard deviation of these measurements, respectively. Black: relative coupling efficiency of an aberrated beam into an FMF matching the entrance geometry of the lantern. Red: similar to the blue points, but the relative proportion of low to high spatial frequency is increased.

experimental testing with the PL, it is hard to determine the precise cause of this discrepancy, which could be due to differences in how the WFE was generated, or due to some intrinsic property of the lantern.

The red points in Figure 4 show how relative throughput of the lantern changes with Strehl, when the proportion of low spatial frequency to high spatial frequency WFE is increased. In the presence of increased low-order error, the throughput no longer behaves linearly, and instead approaches a dependence on Strehl that is more square-root in nature. Qualitatively, this result matches simulations from 5(e.g. Figure 8), though the experimental setup in this work is not completely analogous to the numerical modelling done there. Regardless, both experiment and simulation indicate that higher order aberrations degrade throughput more than lower order aberrations. This is a property of PLs and FMFs in general, which can accept light through a variety of low-order fiber propagation modes, and thus are well-suited to accepting low-order aberrated light.

3.4 Absolute throughput measurement

On July 10, 2022, we took four sets of power meter measurements around the SCExAO IR bench, as described in subsection §2.5. Our results are summarized in Table 1. Conversion of power meter measurements to an absolute throughput value relies on only the first two columns; the third column of data was taken as a consistency check, and for comparison in the event of future power meter measurements. Note that between the two measurement locations corresponding to the first two columns of Table 1, there are also three lenses, one in front and two behind the lantern. The front lens was measured to have a transmission of 0.964; the back lenses are Thorlabs AC080-010-C and AC254-100-C, which together have a theoretical transmission of 0.981. Finally, because the lantern is uncoated, we also must account for Fresnel reflection at the front and back of the lantern. For an interface between air and fused silica, transmission should be 0.96 per surface. This gives the following formula for absolute throughput:

$$\text{absolute throughput} = \frac{\text{power after PL}}{\text{power before lens}} \times \frac{1}{0.964 \times 0.981 \times 0.96^2}. \quad (1)$$

Applying this equation to Table 1 gives an estimated net throughput for the PL of 59±4%. To compare with simulations, numerical models from 5 predict a coupling efficiency into a similarly sized FMF of around 92%: this

sets an upper bound for the coupling efficiency into the PL. Assuming that losses in the PL are predominately internal (occurring as light propagates through the body of the lantern, rather than during coupling into the lantern's entrance) we estimate the internal loss of the lantern to be $1 - 0.59/0.92 = 36\%$. This is significantly higher than our expectation of 5-10%. However, this result is preliminary: future work needs to be done to verify this figure, to separately quantify coupling and internal losses.

Table 1. Power meter measurements (μW).

Before injection lens	After PL	In front of NIR camera
2.00	1.10	0.14
1.97	0.95	0.15
1.78	0.93	0.12
1.61	0.79	0.12

4. DISCUSSION

While our preliminary characterizations of the 19-port PL on the SCExAO bench agree with previous numerical modelling in some areas, they deviate in others. Our next immediate goal will be to determine why these deviations occur. In this section we discuss some possible sources for the discrepancies seen between our experimental results and previous simulations.

The first source to consider is error in the experimental process. As an example, one contributor to the observed discrepancies is our NCPA compensation for the GLINT arm of the SCExAO IR bench. Anecdotally, we note that the impact of NCPA compensation is relatively minor, and often improves relative throughput by 5% or less; additionally our NCPA compensation cannot be too far off since we recover an SMF coupling efficiency similar to previous measurements.[13] As such, imperfect NCPA compensation alone cannot explain the the factor of 3 variations in relative throughput shown in Figure 2, or the mismatch between measured throughput and simulated coupling efficiency at $f/10$ in Figure 3. However, in the future, it would still be prudent to refine our somewhat simplistic NCPA compensation scheme, as outlined in §2.3. Another source of error we are considering is potential angular misalignment between the PL and the optical path: because our injection setup is more sensitive to misalignment when injecting light into waveguides with larger MFDs, misalignment may explain why our coupling efficiency into the SMF is comparatively high, while our measured PL throughput is comparatively low.

Besides experimental error, the other main source for our observed discrepancies between experiment and simulation is that the photonic lantern on the bench is significantly non-ideal. Here, it is important to determine whether this non-ideal-ness is internal, or if it occurs when light enters/exits the lantern. One potential way to disambiguate between the two is to mount a FMF on the injection stage and repeat the characterizations covered in Section §3. Significant differences between the two sets of characterizations might indicate internal imperfections within the lantern. Another useful test might be to reverse-inject light into the PL. This would involve flipping the PL on the injection stage and coupling light into the individual SMF cores at the lantern's MCF end, then imaging the FMF end using the GLINT detector. Measuring the throughput in this manner can help us better characterize PL losses, and can tell us if any of the lantern's cores are underperforming.

The last potential source for our observed discrepancies between experiment and simulation that we will discuss is inaccuracy in previous simulations (e.g. 5). However, we believe this to to be unlikely, since such simulations are based on the physics of coupling into FMFs, which is well-understood. Here, repeating our experimental characterizations with an FMF will again be useful: presuming no issues in the experimental setup, comparisons with the simulated results will confirm or deny the accuracy of the previous simulations.

Finally, we briefly discuss future experiments, after the discrepancies between experiment and simulation have been resolved. The most important test will be to take PLs on sky, so that we can gauge their throughputs in truly realistic conditions. We also plan repeating these characterizations for 3-, 6-, 10-, and 12-port PLs, which will be fabricated at the Sydney Astrophotonic Instrumentation Laboratory (SAIL).

5. CONCLUSION

We presented initial characterizations of the 19-port PL on the SCExAO testbench at Subaru Telescope, and compared these characterizations with simulated results for an FMF that matches the entrance geometry of the lantern. We noted several discrepancies: for one, we find that the experimentally measured throughput of the lantern varies by a factor of up to 3 over the entrance of the lantern, while simulated results suggest coupling efficiency (and hence throughput, for an ideal lantern) should remain relatively flat. Next, we measured PL throughput as a function of focal ratio, and found good agreement with simulations except around a focal ratio of $f/10$. Using the SCExAO turbulence simulator, we then injected WFE into the optical system in order to characterize lantern throughput as a function of Strehl ratio. Our results agree with simulations. Finally, we presented initial results on our measurement of absolute PL throughput. We found a net throughput of $59\pm4\%$; assuming a coupling efficiency of 92%, the upper limit set by simulations, we compute an estimated internal loss for the lantern of 36%. In the future, we plan to extend our characterizations to 3-,6-,10-,and 12-port PLs, and to measure PL throughput on-sky.

ACKNOWLEDGMENTS

This material is based upon work supported by the National Science Foundation Graduate Research Fellowship Program under Grant No. DGE-2034835. This work was also supported by the National Science Foundation under Grant No. 2109232. Any opinions, findings, and conclusions or recommendations expressed in this material are those of the author(s) and do not necessarily reflect the views of the National Science Foundation.

REFERENCES

[1] Bland-Hawthorn, J., Lawrence, J., Robertson, G., Campbell, S., Pope, B., Betters, C., Leon-Saval, S., Birks, T., Haynes, R., Cvetojevic, N., and Jovanovic, N., "PIMMS: photonic integrated multimode microspectrograph," in [*Ground-based and Airborne Instrumentation for Astronomy III*], McLean, I. S., Ramsay, S. K., and Takami, H., eds., *Society of Photo-Optical Instrumentation Engineers (SPIE) Conference Series* **7735**, 77350N (July 2010).

[2] Jovanovic, N., Schwab, C., Cvetojevic, N., Guyon, O., and Martinache, F., "Enhancing stellar spectroscopy with extreme adaptive optics and photonics," *Publications of the Astronomical Society of the Pacific* **128**, 121001 (nov 2016).

[3] Leon-Saval, S. G., Birks, T. A., Bland-Hawthorn, J., and Englund, M., "Multimode fiber devices with single-mode performance," *Opt. Lett.* **30**, 2545–2547 (Oct 2005).

[4] Birks, T. A., Gris-Sánchez, I., Yerolatsitis, S., Leon-Saval, S. G., and Thomson, R. R., "The photonic lantern," *Adv. Opt. Photon.* **7**, 107–167 (Jun 2015).

[5] Lin, J., Jovanovic, N., and Fitzgerald, M. P., "Design considerations of photonic lanterns for diffraction-limited spectrometry," *J. Opt. Soc. Am. B* **38**, A51–A63 (Jul 2021).

[6] Leon-Saval, S. G., Fontaine, N. K., and Amezcua-Correa, R., "Photonic lantern as mode multiplexer for multimode optical communications," *Optical Fiber Technology* **35**, 46–55 (2017). Next Generation Multiplexing Schemes in Fiber-based Systems.

[7] Martinez, P., Loose, C., Aller Carpentier, E., and Kasper, M., "Speckle temporal stability in xao coronagraphic images," *A&A* **541**, A136 (2012).

[8] Martinez, P., Kasper, M., Costille, A., Sauvage, J. F., Dohlen, K., Puget, P., and Beuzit, J. L., "Speckle temporal stability in xao coronagraphic images - ii. refine model for quasi-static speckle temporal evolution for vlt/sphere," *A&A* **554**, A41 (2013).

[9] N´Diaye, M., Martinache, F., Jovanovic, N., Lozi, J., Guyon, O., Norris, B., Ceau, A., and Mary, D., "Calibration of the island effect: Experimental validation of closed-loop focal plane wavefront control on subaru/scexao," *A&A* **610**, A18 (2018).

[10] Vievard, S., Bos, S., Cassaing, F., Ceau, A., Guyon, O., Jovanovic, N., Keller, C. U., Lozi, J., Martinache, F., Montmerle-Bonnefois, A., Mugnier, L., NDiaye, M., Norris, B., Sahoo, A., Sauvage, J.-F., Snik, F., Wilby, M. J., and Wong, A., "Overview of focal plane wavefront sensors to correct for the low wind effect on subaru/scexao," (2019).

[11] Ahn, K., Guyon, O., Lozi, J., Vievard, S., Deo, V., Skaf, N., Belikov, R., Bos, S. P., Bottom, M., Currie, T., Frazin, R., Gorkom, K. V., Groff, T. D., Haffert, S. Y., Jovanovic, N., Kawahara, H., Kotani, T., Males, J. R., Martinache, F., Mazin, B., Miller, K., Norris, B., Rodack, A., and Wong, A., "SCExAO: a testbed for developing high-contrast imaging technologies for ELTs," in [*Techniques and Instrumentation for Detection of Exoplanets X*], Shaklan, S. B. and Ruane, G. J., eds., **11823**, 9 – 21, International Society for Optics and Photonics, SPIE (2021).

[12] Guyon, O., "Phase-induced amplitude apodization of telescope pupils for extrasolar terrestrial planet imaging," *A & A* **404**(1), 379–387 (2003).

[13] Jovanovic, N., Schwab, C., Guyon, O., Lozi, J., Cvetojevic, N., Martinache, F., Leon-Saval, S., Norris, B., Gross, S., Doughty, D., Currie, T., and Takato, N., "Efficient injection from large telescopes into single-mode fibres: Enabling the era of ultra-precision astronomy," *A & A* **604**, A122 (2017).

[14] Martinod, M.-A., Norris, B., Tuthill, P., Lagadec, T., Jovanovic, N., Cvetojevic, N., Gross, S., Arriola, A., Gretzinger, T., Withford, M. J., Guyon, O., Lozi, J., Vievard, S., Deo, V., Lawrence, J. S., and Leon-Saval, S., "Scalable photonic-based nulling interferometry with the dispersed multi-baseline glint instrument," *Nature Communications* **12**, 2465 (Apr 2021).

[15] Trinh, C. Q., Ellis, S. C., Bland-Hawthorn, J., Lawrence, J. S., Horton, A. J., Leon-Saval, S. G., Shortridge, K., Bryant, J., Case, S., Colless, M., Couch, W., Freeman, K., Löhmannsröben, H.-G., Gers, L., Glazebrook, K., Haynes, R., Lee, S., O'Byrne, J., Miziarski, S., Roth, M. M., Schmidt, B., Tinney, C. G., and Zheng, J., "GNOSIS: The first instrument to use fiber Bragg gratings for OH suppression," *The Astronomical Journal* **145**, 51 (jan 2013).

[16] Leon-Saval, S. G., Fontaine, N. K., Salazar-Gil, J. R., Ercan, B., Ryf, R., and Bland-Hawthorn, J., "Mode-selective photonic lanterns for space-division multiplexing," *Opt. Express* **22**, 1036–1044 (Jan 2014).

APPENDIX A. CONVERSION OF INJECTION STAGE POSITION TO FOCAL RATIO

For two converging lenses separated by some distance d, the formula for equivalent focal length (and hence focal ratio F) will take the form

$$F(d) = \frac{1}{a + bd} \tag{2}$$

for real-valued constants a and b. In the context of SCExAO, we instead have an OAP (see OAP6, Figure 1) and a convex lens, but the physics is the same. Separation between the OAP and the lens is linearly related to the optical carriage position z, so that focal ratio F also has the dependence $F(z)$ as described by equation 2. To determine the best values for a and b, we measured the coupling efficiency into the SMF on the injection stage, denoted $C_e(z)$ as a function of z. This data was provided by Sebastien Vievard. We also numerically computed the theoretical SMF coupling efficiency as a function of focal ratio F, denoted $C_s(F)$ and plotted in blue in Figure 5. Finally, we used a Nelder-Meade optimizer to find the values of a and b which minimized the squared residual between $C_e(z)$ and $C_s(F(z))$ over an array of z values. This gives the best-fit relation $F(z)$, plotted in the right panel of Figure 5. The experimentally measured values of SMF coupling, plotted against focal ratio instead of z using the best-fit transformation $F(z)$, is shown by the black points in Figure 5, left. These points agree well with simulation.

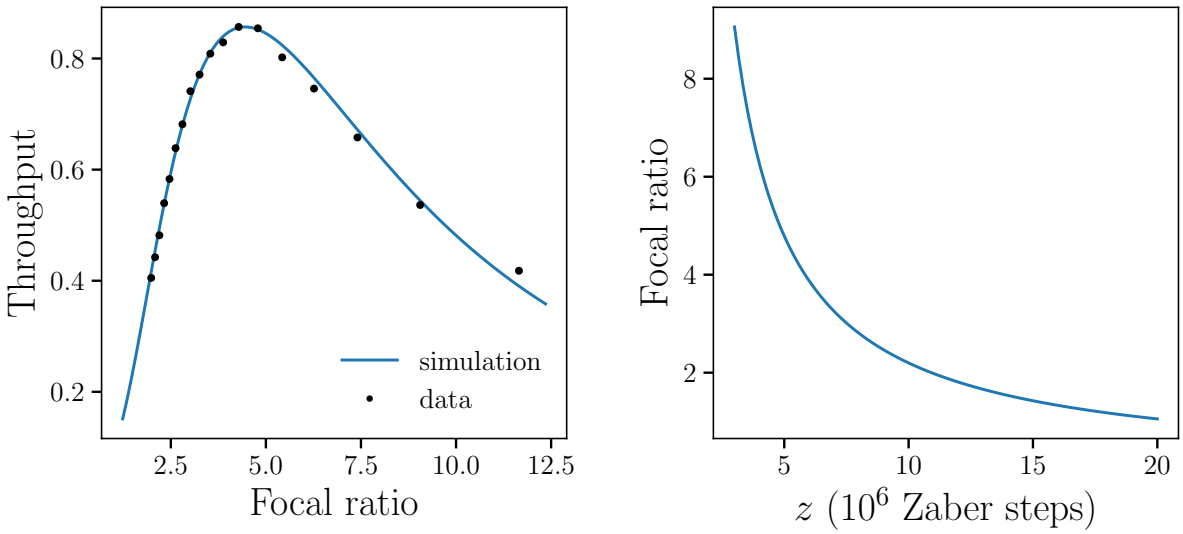

Figure 5. Left: comparison of simulated SMF coupling and experimentally measured coupling, after applying our best-fit transformation $F(z)$ to the carriage position coordinate z. Right: best-fit relation for $F(z)$.